Iranian Journal of Materials Science and Engineering, Vol. 21, Number 1, March 2024
RESEARCH PAPER

Structural, Optical, and Supercapacitive Properties of Pure, Nickel, and Molybdenum Ion Doped Trimanganese Tetraoxide (Mn_3O_4) Thin Films

Tanaji. S. Patil[1,*], S. M. Nikam[1], R. S. Kamble[2], R. B. Patil[3], M. V. Takale[4], S. A. Gangawane[5,*]

* *tanajipatil11@gmail.com, gangawane.satish98@gmail.com*

[1] Department of Physics, Bhogawati Mahavidyalaya, Kurukali, Shivaji University Kolhapur, Maharashtra, India
[2] Department of Chemistry, Bhogawati Mahavidyalaya, Kurukali, Shivaji University Kolhapur, Maharashtra, India
[3] Department of Physics, Shri. Yashwantrao Patil Science College Solankur, Shivaji University Kolhapur, Maharashtra, India
[4] Department of Physics, Shivaji University Kolhapur, Maharashtra, India
[5] Department of Physics, Doodhsakhar Mahavidyalaya Bidri, Shivaji University Kolhapur, Maharashtra, India

Received: December 2023 **Revised: March 2024** **Accepted: March 2024**
DOI: 10.22068/ijmse.3527

Abstract: *The trimanganese tetraoxide (Mn_3O_4) nanostructured thin films doped with 2 mol% of nickel (Ni) and molybdenum (Mo) ions were deposited by a simple electrophoretic deposition technique. The structural, optical, and morphological studies of these doped thin films were compared with pure Mn_3O_4 thin films. X-ray diffraction (XRD) confirmed the tetragonal Hausmannite spinel structure. The Fourier transform infrared spectroscopy (FTIR) provided information about the molecular composition of the thin films and the presence of specific chemical bonds. The optical study and band gap energy values of all thin films were evaluated by the UV-visible spectroscopy technique. The scanning electron microscopy (SEM) illustrated the morphological modifications of the Mn_3O_4 thin films due to doping of the nickel and molybdenum ions. The Brunauer Emmett Teller (BET) method has confirmed the mesoporous nanostructure and nanopores of the thin films. The supercapacitive performance of the thin films was studied by cyclic voltammetry (CV), and galvanostatic charge discharge (GCD) techniques using the three-electrode arrangement. An aqueous 1M Na_2SO_4 electrolyte was used for the electrochemical study. The 2 mol% Ni-doped Mn_3O_4 thin film has shown maximum specific capacitance than pure and Mo-doped Mn_3O_4 thin films. Hence, this study proved the validity of the strategy - metal ion doping of Mn_3O_4 thin films to develop it as a potential candidate for electrode material in futuristic energy storage and transportation devices.*

Keywords: *Electrophoretic deposition, Doping by metal ions, Mesoporous, Pseudocapacitors.*

1. INTRODUCTION

Greater energy density, highly reversible, exceptional cyclic life, and potential to transport high power are the key aspects that attracted the researchers towards the supercapacitors [1, 2]. Metal oxides were widely used as electrodes in various energy storage devices which were reported earlier. RuO_2 and IrO_2 are the popular oxide nanomaterials employed as electrode materials, but their applicability was limited due to their high cost and complicated synthesis. Other oxides such as vanadium, iron, manganese, and copper were also studied [3, 4], but lower cost, higher availability, great stability, and environment-friendly nature are the key parameters of manganese oxide as a fascinating and emerging nanomaterial. Among other oxides of manganese, the Hausmannite Mn_3O_4 is the most stable and frequently used nanomaterial. Due to a variety of morphologies and different oxidation states, the spinel Mn_3O_4 nanomaterial has wide applications like sensors, catalysts, batteries, ion exchange, and supercapacitors. Many reports on its physical and chemical synthesis are available [5, 6, 7, 8].

Here, the most versatile electrophoretic deposition technique is used to deposit the thin films, in which the stoichiometry of the depositing layer can be controlled easily and deposited on a larger area with a low-cost apparatus. In it, the ionic particles are dispersed in the suspension, moved by the electric force, and deposited on an oppositely charged electrode by applying a DC voltage [9]. The uniformity and thickness of thin films were affected by parameters like temperature, pH, concentration, and applied potential [10]. Many reports were available on morphology, size, and crystallinity-dependent optical, supercapacitive, and catalytic properties of Mn_3O_4 nanomaterials [11]. Thus, the doping of metal ions is a fruitful strategy to modify these properties of nanomaterials. Especially, the metallic atoms having comparable

[DOI: 10.22068/ijmse.3527]

radius with depositing materials atoms can alter the properties and morphology by occupying different positions in the nanostructure. Various doping metal ions such as Fe, Li, Co, Cr, and Ni are reported [12, 13, 14], however, very few reports are available on the doping of Ni and Mo ions in the Mn_3O_4 nanostructure [15, 16].

In this work, nickel and molybdenum are the dopants, due to their larger availability, low cost, and radius comparable with manganese. Therefore, they can easily substitute the Mn ions in the Mn_3O_4 spinel nanostructure. Here, the XRD, FTIR, UV visible, SEM, and BET studies of pure, 2 mol% Ni, and 2 mol% Mo doped Mn_3O_4 thin films are executed. Also, how the Ni and Mo ion doping enhances the supercapacitive performance of the Mn_3O_4 thin films is examined.

2. EXPERIMENYAL PROCEDURES

2.1. Materials

Manganese sulfate hexahydrate ($MnSO_4 \cdot 7H_2O$), hexamine (HMTA) ($(CH_2)_6N_4$), sodium sulphate (Na_2SO_4), nickel nitrate ($Ni(NO_3)_2 \cdot 6H_2O$), ammonium molybdate $(NH_4)_6Mo_7O_{24}$ and ammonia (NH_3) were of analytical grade purchased from Thomas Baker India Pvt. Ltd and used without any further purification.

2.2. Electrophoretic Deposition of Thin Films

For electrophoretic deposition of the pure Mn_3O_4 thin films on a stainless-steel (SS) electrode, 50 ml of 0.05 M $MnSO_4$ and 50 ml 0.05 M HMTA solutions were prepared using double distilled water and both stirred for 30 minutes. Then, both solutions were mixed and an appropriate amount of ammonia was added for the whitish-yellow precipitation and stirred vigorously for 120 minutes. Later, the well-cleaned SS and graphite electrodes were vertically immersed in the above solution.

The constant potential of value 1.1 Volts was applied across the electrodes for 30 minutes to deposit a well-adherent thin film of Mn_3O_4 which was denoted by M. These thin films were dried at room temperature in air. By the same procedure, the Ni and Mo-doped Mn_3O_4 thin films were deposited at a temperature of 343°K by adding 2 mol% of nickel nitrate and ammonium molybdate in the $MnSO_4$ solution. These doped dark black colored Mn_3O_4 thin films were indicated as MM and MN [17, 18].

2.3. Characterizations

For the crystal system information, the thin films were analyzed by x-ray diffractometer (XRD, AXS DS Advance, Bruker) having Cu-Kα radiation of x-ray with a scanning rate of value 2°/min. The Debye-Scherrer formula was used to find crystallite size (D).

$$D = \frac{0.9\lambda}{\beta\cos\theta} \quad (1)$$

Where k - 0.9 is known as the shape factor, λ = 0.1541 nm - the wavelength of Cu-kα x-rays, β - FWHM (in radian) of peak, and θ – the angle of diffraction. With the help of FTIR spectroscopy (ALPHA, Bruker, Germany), the study of the FTIR spectrum of thin films in the range of 400–4000 cm^{-1} was executed. A UV visible NIR DRS Spectrophotometer (V770, Jasco, Japan) was used for optical study and band gap determination of the thin films. The morphology of the surface of the thin films was captured with the SEM equipment (JEOL, JSM-IT200). The BET-Surface area analyzer is employed for the measurement of surface area and pore size of nanostructured thin films. The CHI660E workstation was employed for the evaluation of the electrochemical performances. For it, a three-electrode cell arrangement was used in which the deposited thin film was the working electrode, Pt wire was the counter electrode, and saturated calomel electrode (SCE) was the reference electrode.

3. RESULTS AND DISCUSSION

3.1. X-ray Diffraction Studies

The X-ray diffraction patterns for pure, Ni, and Mo-doped Mn_3O_4 thin films are shown in Fig. 1. All the peaks in the diffraction pattern were indexed according to JCPDS card no. 01-1127, space group I41/amd confirms the spinel tetragonal Haumannite structure of Mn_3O_4 [17-19]. As the peaks of any impurity are not observed it approves the suitability of the electrophoretic deposition technique for the deposition of nanostructured thin films. The crystallinity of the Mn_3O_4 thin films reduces due to metal ion doping. The Mo-doped thin films have lower crystallinity than the Ni-doped and pure Mn_3O_4 thin films which is indicated by low intense peaks in their diffraction patterns. As the ionic radius of Mo is smaller than Mn and Ni, the intensity of peaks in its diffraction pattern reduces due to the formation

[DOI: 10.22068/ijmse.3527]

of disarrangements in the Mn_3O_4 structure due to the presence of Mo ions [20]. The Debye-Scherrer relation is used to evaluate average crystallite size (D), and hence the dislocation energy (δ) and microstrain (ε) are also evaluated [21]. The structural study reveals that the average crystallite size increases while dislocation density and microstrain decrease for Mo-doped thin film than pure Mn_3O_4 thin film and average crystallite size, dislocation density, and microstrain are decreased for Ni-doped thin film, which is displayed in Table 1.

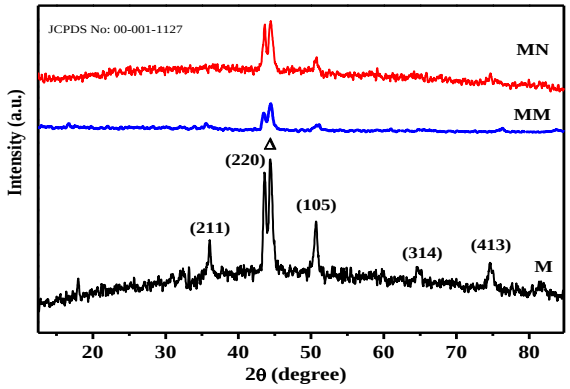

Fig. 1. XRD patterns of MN, MM, M thin film [17, 18].

Table 1. Structural Parameters of M, MM, and MN thin films.

Thin films	Average crystallite size (nm)	Dislocation density (δ) x 10^{15} m^{-2}	Micro strain (ε)
M	152	0.432	0.1248
MM	182	0.301	0.1052
MN	76	1.732	0.1027

3.2. FTIR Studies

FTIR spectra, studied in the wavenumber range 400 to 4000 cm^{-1} for MN, MM, and M thin films are illustrated in Fig. 2. The intense absorption peaks at 410, 520, and 620 cm^{-1} signify the stretched vibrations of Mn-O at octahedral and tetrahedral sites of the Mn_3O_4 nanostructure. The bending vibrations of O-H in locked moisture in the MM thin film are represented by the peak at 1620 cm^{-1}. The presence of Mo and Ni is identified by FTIR spectra containing reduced intense peaks. The slight shifting of all Mn-O peaks in the case of MM and MN thin films indicates the replacement of dopant ions in the tetrahedral place of Mn ions [22]. The decrease in intensity of these peaks is due to variations in the amplitude of the vibratory motion of Mn ions that are vibrating at their natural frequency due to incident radiation in the presence of the dopant ions [23].

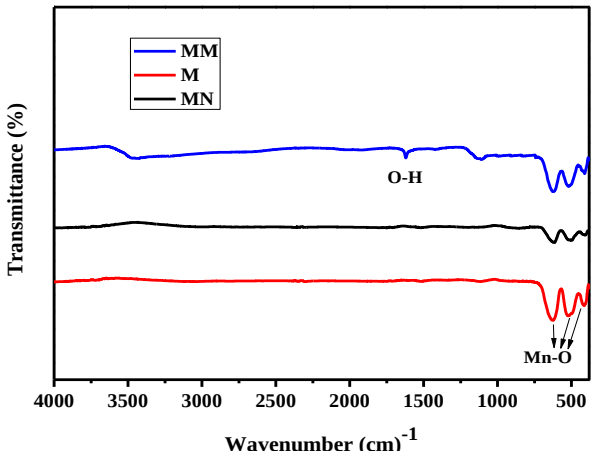

Fig. 2. FTIR spectra of MM, M, MN thin films.

3.3. UV Visible Spectroscopy

The UV-visible absorption spectra (Absorbance vs. Wavelength) of MM, M, and MN thin films are shown in Fig. 3 a). It contains two absorption peaks at 258 nm, and 294 nm for M, MM, and MN thin films due to highly energetic Mn^{2+}/Mn^{3+} interactions. The low intense peak at wavelengths 425, 410, and 470 nm of M, MM, and MN thin films indicate the d-d transitions of Mn^{3+} ions which is explained by the Jahn–Teller effect [24]. At higher wavelengths, the absorption decreases for all thin films with the least absorption for MM and higher absorption for MN thin film. The graph of $(\alpha h\upsilon)^2$ versus the energy of the photon ($h\upsilon$) for the MM, M, and MN thin films is shown in Fig. 3b) and is useful to calculate band gap energy with the help of the Tauc equation [25].

$$(\alpha h\upsilon) = A\,(Eg - h\upsilon)^n \quad (2)$$

With absorption coefficient (α), band gap energy (Eg), and a constant (A) with n values 1/2 and 2 representing direct and indirect transitions. The linear curve signifies the direct band gap of the values 3.26 eV for M, and 3.30 eV for MM and MN thin films due to the quantum confinement effect [26]. This slightly increased band gap energy due to doping of Mo and Ni ions causes an improvement in their conductivity and hence their supercapacitive behavior. These observed band gap values also signify the suitability of these thin films in optoelectronic types of equipment such as LEDs.

[DOI: 10.22068/ijmse.3527]

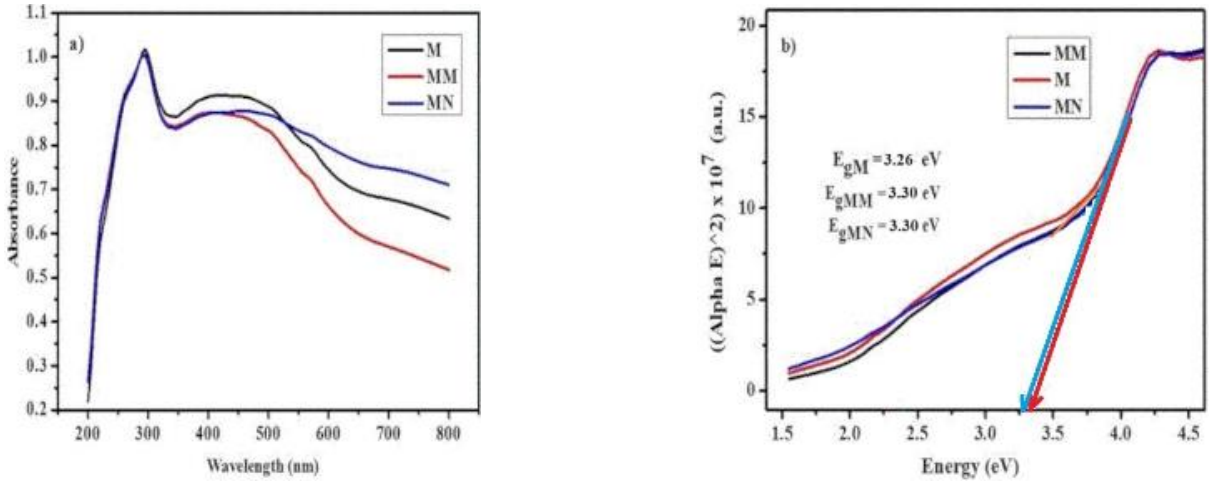

Fig. 3. a) Optical absorption spectra, b) Band gap energy diagram of MM, M, and MN thin films.

3.4. Scanning Electron Microscopy (SEM)

Morphology of the nanostructure is a crucial aspect that affects the electrochemical performance of thin films. SEM images illustrated in Fig. 4 a), b), and c) represent the morphology of the surface of nanostructured M, MM, and MN thin films. The SEM image of the M thin film illustrates the grass-like nanostructure of random orientation with grain size or average crystallite size of 150 nms.

The MM thin film has porous and spongy nanostructure having a grain size or average crystallite size in the range of 150-200 nms and the MN thin film has interrelated nanoflake morphology with greater porosity but decreased grain size or average crystallite size of value of 100 nms. Thus, the morphology and porosity alteration in the Mn3O4 thin film due to the doping of Mo and Ni ions causes enhanced supercapacitive performance [24].

3.5. Brunauer-Emmett-Teller (BET)

Fig. 5 a) shows the nitrogen adsorption/ desorption isotherms of the M, MM, and MN thin films and Fig. 5 b) displays their pore size distribution curves obtained from the desorption isotherms. These nitrogen isotherms are of type IV, confirm the of all thin films and are observed in the range of 0.3 to 1 P/P_0 [27]. Table 2 illustrates the BET specific surface area, pore volume, and pore size of the pure M, MM, and MN thin films. It elucidates the effect of dopant on the porosity of Mn_3O_4 nanostructured thin films. The surface area is almost doubled in both doped (MM and MN) thin films than in pure (M) thin films. The pore volume decreases to nearly a partial amount for MN thin film and increases doubly for MM thin film than the pure M thin film. The value of pore size slightly increases for MM thin film and decreases almost to one third value for MN thin film than that of the pure M thin film.

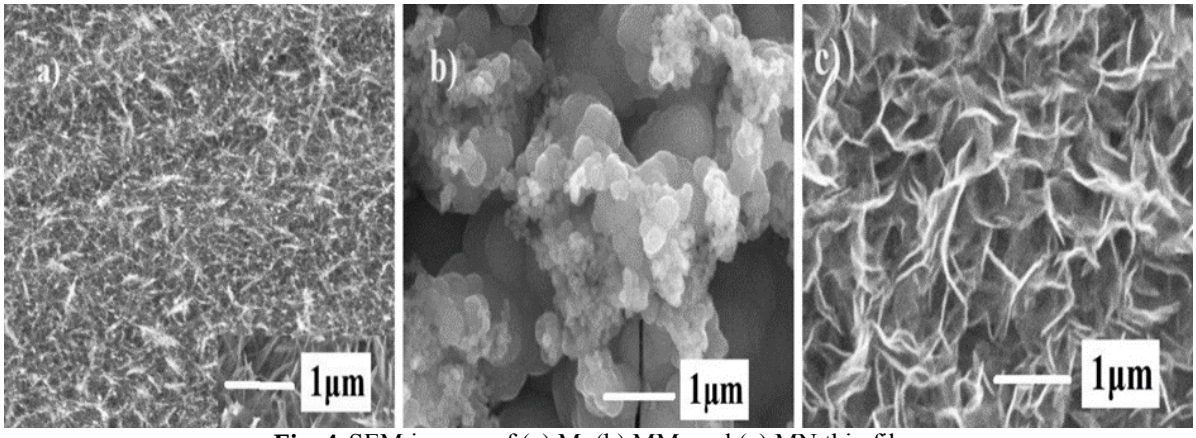

Fig. 4. SEM images of (a) M, (b) MM, and (c) MN thin film.

[DOI: 10.22068/ijmse.3527]

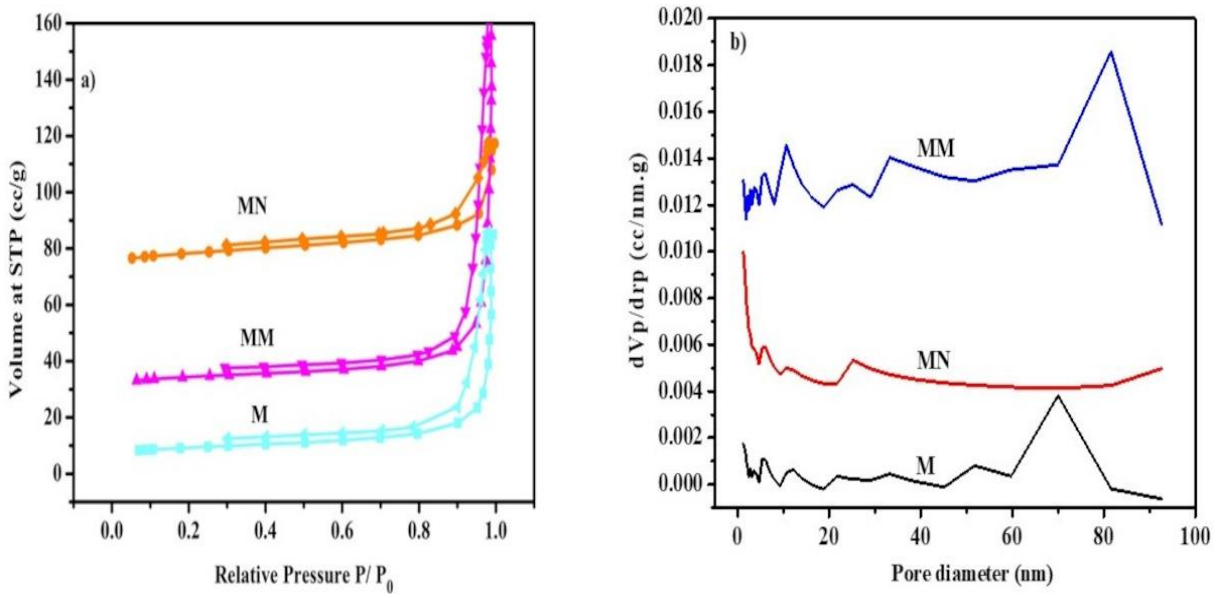

Fig. 5. a) Nitrogen adsorption/desorption isotherms, b) pore size distribution of the MM, MN, and M thin films.

Table 2. BET Parameters M, MM, and MN thin films.

Thin films	Surface area (m^2 g^{-1})	Pore volume (cm^3 g^{-1})	Pore size (nm)
M	12.77	0.12	32.39
MM	27.26	0.2855	41.49
MN	27.47	0.068	10.08

Thus, all BET parameters reveal that the doped Mn_3O_4 thin films have higher porosity and surface area than the pure Mn_3O_4 thin film [28], which becomes beneficial for charge transportation and enhanced supercapacitive performance.

3.6. Supercapacitive Studies

3.6.1. Cyclic voltammetry studies

It is an important electrochemical feature to estimate the electrochemical performance of thin film electrodes. Fig. 6 a) to d) illustrates the cyclic voltammetry (CV) curves of MN, MM, and M thin films at different scan rates of 10, 20, 50, and 100 mV s^{-1}. The quasi-rectangular nature of the CV curve shows both electrochemical double-layer capacitive and pseudocapacitive behavior for pure M thin films. Almost rectangular shapes of CV curves with some smaller redox peaks for MM and MN thin films represent their exceptional pseudocapacitive nature due to the rapid, repetitive, and consecutive redox reactions at the surface by the adsorption of electrolyte cations. Also, some extent of charge storage occurs at the interface of the electrode–electrolyte by the formation of an electric double layer that confirms the synergistic effect between the dopant and Mn_3O_4 nanostructure [29]. The CV curves of the MN thin film electrode enclose a larger area and hence have a higher surface-to-volume ratio due to increased electrochemically active centers on the surface which is responsible for the subsequent improvement in the specific capacitance. Also, its narrow pores provide a more stable structure for ion intercalation/ removal into/out forming a double layer. The MM thin film electrode also shows an excellent supercapacitive performance, since it has a smaller surface area and porosity than the MN thin film but larger than the M thin film electrode. The shape of CV curves for all thin films changes with increasing scan rate due to lowered electrochemical activities by creating active sites in the presence of electrolytic ions [27].

3.6.2. Galvanostatic charge/discharge studies

The electrochemical study of the electrophoretically deposited M, MM, and MN thin film electrode is carried out by the galvanostatic charge/discharge method in the potential range 0 to 0.7 V vs. SCE at different current density values. Fig. 7 illustrates the charge/discharge curves recorded at current densities of 0.3 and 1 A g^{-1}. It elucidates the nearly symmetrical charge-discharge curves and confirms an excellent pseudocapacitive behavior due to surface.

[DOI: 10.22068/ijmse.3527]

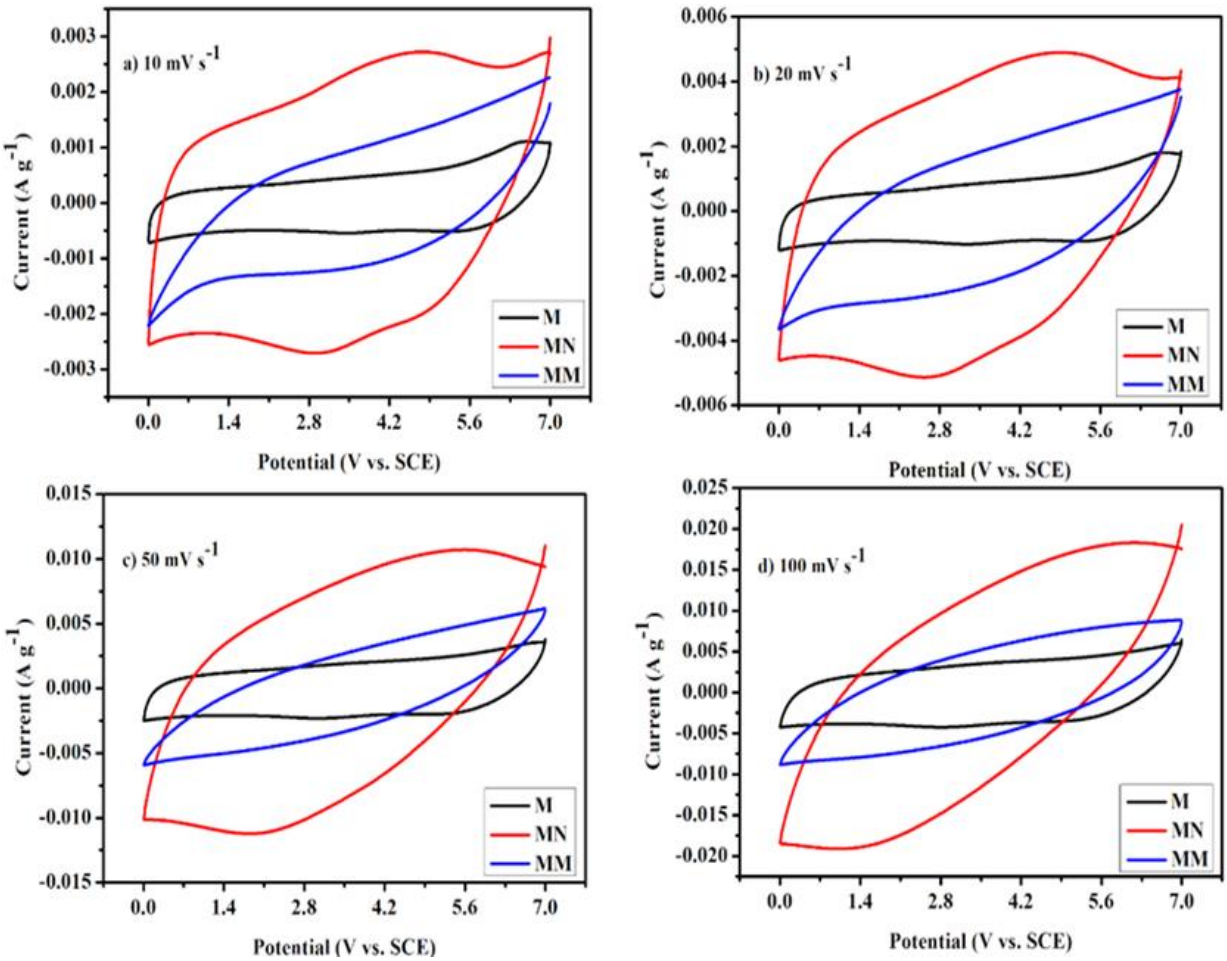

Fig. 6. The cyclic voltammetry curves of MN, MM, and M thin films at scan rates a) 10, b) 20, c) 50, and d) 100 mV s^{-1}.

Redox reactions in mesoporous nanostructured thin films [20]. Due to narrow pores and high surface area, the MN and MM thin films exhibit an excellent supercapacitive performance than the M thin film electrode.

Table 3. The specific capacitance values of nanostructured M, MM, and MN thin film electrodes.

Thin films	Current density (A g^{-1})	Specific capacitance (F g^{-1})
M	0.3	172
	1	142
MM	0.3	414
	1	338
MN	0.3	720
	1	630

By analyzing discharge curves and using equation 3, the specific capacitance values of nanostructured MM, MN, and M thin film electrodes are determined and shown in Table 3.

$$Cs = i\ \Delta V / m\ \Delta t \quad (3)$$

Where i - the discharge current (A), ΔV - the potential window (V), Δt - the discharging time (s), and m - the mass of the deposited materials in the electrodes (g cm^{-2}).

Thus, the MN and MM thin film electrodes have higher specific capacitance values than the M thin film electrode due to the larger accessible surface area, enhanced electrical conductivity, and surface redox reactions [30, 31].

4. CONCLUSIONS

In summary, the pure, 2 % Mo and Ni doped Mn_3O_4 thin films were deposited on a stainless-steel substrate via an easy and cheap electrophoretic deposition technique and an enhanced supercapacitive was observed for the Ni and Mo doped Mn_3O_4 thin films. The XRD analysis showed that all thin films have a

[DOI: 10.22068/ijmse.3527]

tetragonal Hausmannite spinel structure.

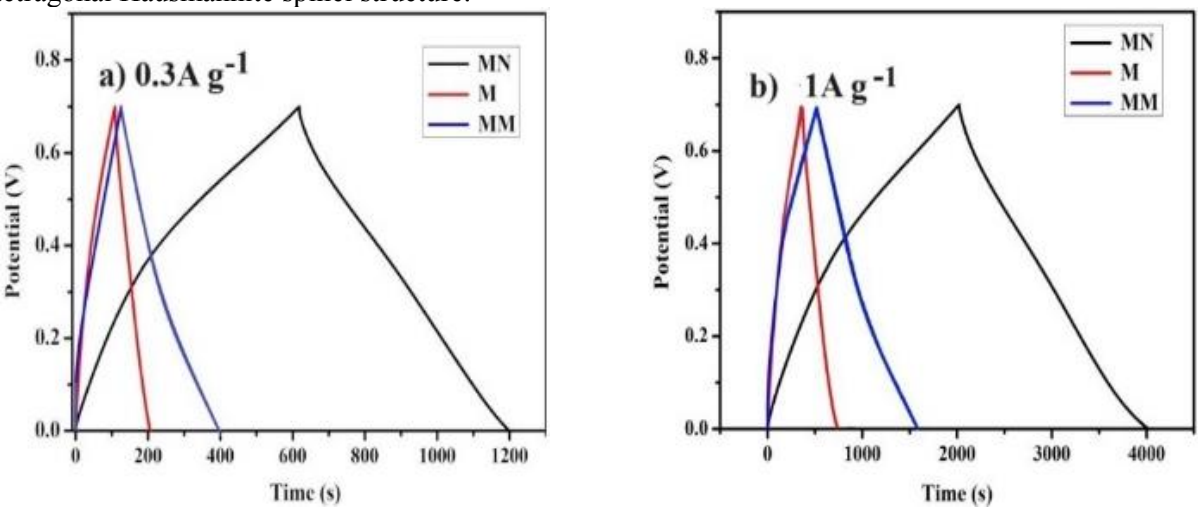

Fig. 7. The galvanostatic charge-discharge curves of M, MN, and MM thin films at current densities of 0.3 and 1 A g^{-1}.

The average crystallite size and microstrain increase for Mo-doped and decrease for Ni-doped thin films while the dislocation density decreases for Mo-doped and increases for Ni-doped thin films than pure Mn_3O_4 thin film. FTIR studies showed the impurity-free deposition of pure, Ni, and Mo-doped Mn_3O_4 films. The UV visible spectroscopy measurements of all thin films have shown identical optical properties but greater band gap energy values due to the presence of dopant. The surface morphological change was also observed due to doping which was confirmed by the SEM studies. The pure thin films have nanowire-like structures, Ni-doped thin films have nanoflake structures while the Mo-doped thin films have nanostructured structures. BET analysis elucidated that Ni-doped thin film has narrow pores, higher porosity, and surface area than
Mo-doped and pure Mn_3O_4 thin films. Supercapacitive studies elucidated a larger specific capacitance of value 720 F g^{-1} for Ni-doped Mn_3O_4 thin film and 374 F g^{-1} for Mo-doped Mn_3O_4 thin film than the pure Mn_3O_4 thin film. Due to features such as affordability, easy synthesis with morphological tuning, and excellent supercapacitive performance, the doped Mn_3O_4 thin films could be a promising candidate to use as electrodes in energy storage and transportation devices.

ACKNOWLEDGMENT

The authors are thankful to the Coordinator, Sophisticated Analytical Instrument Facilities (SAIF) center, Shivaji University Kolhapur, CFC-Devchand College Arjunnagar, Nipani, CFC-Y.C. Institute of Science, Satara, CFC- Jaysingpur college, Jaysingpur, and Department of Physics, Shivaji University, Kolhapur for providing the characterization facilities to carry out this research work in a successful manner.

CREDIT AUTHORSHIP CONTRIBUTION STATEMENT

Tanaji S. Patil: Synthesis, characterizations, and writing; S. M. Nikam: Synthesis; R. S. Kamble: Writing - review and editing; R. B. Patil, M. V. Takale, S.A. Gangawane: Supervision. All authors read and approved the final manuscript.

DECLARATION OF COMPETING INTEREST.

There are no conflicts to declare.

REFERENCES

[1]. Gautham Prasad, G., Shetty, N., Thakur, S., Rakshitha, & Bommegowda, K. B. Supercapacitor technology and its applications: A review. IOP Conference Series: Materials Science and Engineering, 2019, 561(1). https://doi.org/10.1088/1757-899X/561/1/012105.

[2]. Şahin, M., Blaabjerg, F., & Sangwongwanich, A. A Comprehensive Review on Supercapacitor Applications

[DOI: 10.22068/ijmse.3527]

and Developments. Energies, 2022, 15(3), 674. https://doi.org/10.3390/en15030674.

[3]. Liang, R., Du, Y., Xiao, P., Cheng, J., Yuan, S., Chen, Y., Yuan, J. and Chen, J. Transition metal oxide electrode materials for supercapacitors: a review of recent developments. Nanomaterials, 2021, 11(5), 1248. https://doi.org/10.3390/nano11051248.

[4]. An, C., Zhang, Y., Guo, H., & Wang, Y. Metal oxide-based supercapacitors: progress and prospectives. In Nanoscale Advances 2019, 1(12), 4644–4658). Royal Society of Chemistry. https://doi.org/10.1039/c9na00543a.

[5]. Chen, C., Ding, G., Zhang, D., Jiao, Z., Wu, M., Shek, C. H., Wu, C. M. L., Lai, J. K. L., & Chen, Z. Microstructure evolution and advanced performance of Mn_3O_4 nanomorphologies. Nanoscale, 2012, 4(8), 2590–2596. https://doi.org/10.1039/c2nr12079h.

[6]. Gnana, B., Raj, S., Asiri, A. M., Wu, J. J., & Anandan, S. Synthesis of Mn_3O_4 Nanoparticles via Chemical Precipitation Approach for Supercapacitor Application. Jj.Alloys and Compounds,. 2015, https://doi.org/10.1016/j.jallcom.2015.02.164.

[7]. Cao, S., Han, T., Peng, L., & Liu, B. Hydrothermal preparation, formation mechanism and gas-sensing properties of novel Mn_3O_4 nano-octahedrons. Materials Letters, 2019, 246, 210–213. https://doi.org/10.1016/j.matlet.2019.02.127.

[8]. Yang, Y., Huang, X., Xiang, Y., Chen, S., Guo, L., Leng, S., & Shi, W. Mn_3O_4 with different morphologies tuned through one-step electrochemical method for high-performance lithium-ion batteries anode. Journal of Alloys and Compounds, 2019, 771, 335–342. https://doi.org/10.1016/j.jallcom.2018.08.328.

[9]. Park, Y., Kang, H., Jeong, W., Son, H., & Ha, D.-H. Electrophoretic Deposition of Aged and Charge Controlled Colloidal Copper Sulfide Nanoparticles. Nanomaterials, 2021, 11(1), 133. https://doi.org/10.3390/nano11010133.

[10]. Sarkar, P., & Nicholson, P. S. Electrophoretic deposition (EPD): Mechanisms, kinetics, and application to ceramics. In Journal of the American Ceramic Society 1996, 79(8), 1987–2002. https://doi.org/10.1111/j.1151-2916.1996.tb08929.x.

[11]. Sukhdev, A., Challa, M., Narayani, L., Manjunatha, A. S., Deepthi, P. R., Angadi, J. V., Mohan Kumar, P., & Pasha, M. Synthesis, phase transformation, and morphology of hausmannite Mn_3O_4 nanoparticles: photocatalytic and antibacterial investigations. Heliyon, 2020, 6(1), e03245. https://doi.org/10.1016/j.heliyon.2020.e03245.

[12]. Almontasser, A., & Parveen, A. Probing the effect of Ni, Co and Fe doping concentrations on the antibacterial behaviors of MgO nanoparticles. In Scientific Reports. Nature Publishing Group UK. 2022, 12(1), 7922. https://doi.org/10.1038/s41598-022-12081-z.

[13]. Zhang, X., Xu, Y., Li, D., & Zhang, Y. The effect of metal ions doping on the electrochemical performance of molybdenum trioxide. Electrochimica Acta, 2018, 283, 149–154. https://doi.org/10.1016/j.electacta.2018.06.166.

[14]. Iqbal, M., Ali, A., Ahmad, K. S., Rana, F. M., Khan, J., Khan, K., & Thebo, K. H. Synthesis and characterization of transition metals doped CuO nanostructure and their application in hybrid bulk heterojunction solar cells. SN Applied Sciences, 2019, 1(6), 1–8. https://doi.org/10.1007/s42452-019-0663-5.

[15]. Patra, T., Panda, J., & Sahoo, T. R. Modification of structural, optical, and dielectric properties of Mn_3O_4 NPs by doping of Nickel ions. Journal of Materials Science: Materials in Electronics, 2023, 34(15), 1224. https://doi.org/10.1007/s10854-023-10624-2.

[16]. Naiknaware, A. G., Chavan, J. U., Kaldate, S. H., & Yadav, A. A. Studies on spray deposited Ni doped Mn_3O_4 electrodes for supercapacitor applications. Journal of Alloys and Compounds, 2019, 774, 787–794. https://doi.org/10.1016/j.jallcom.2018.10.

[DOI: 10.22068/ijmse.3527]

001.

[17]. Patil, T. S., Kothavale, V. P., Malekar, V. P., Kamble, R. S., Patil, R. B., Gurav, K. V., Takale, M. V., & Gangawane, S. A. Effect of Nickel (Ni) Ion Doping on the Morphology and Supercapacitive Performance of Mn_3O_4 Thin Films. Journal of Electronic Materials, 2024, 53(1), 394–407. https://doi.org/10.1007/s11664-023-10765-4.

[18]. Patil, T. S., Kamble, R. S., Patil, R. B., Takale, M. V., & Gangawane, S. A. Enhanced supercapacitive performance of electrophoretically deposited nanostructured molybdenum-doped Mn_3O_4 thin films. International Journal of Materials Research. 2023. https://doi.org/10.1515/ijmr-2022-0414.

[19]. Liu, Z., Zhang, L., Xu, G., Zhang, L., Jia, D., & Zhang, C. Mn_3O_4 hollow microcubes and solid nanospheres derived from a metal formate framework for electrochemical capacitor applications. RSC Advances, 2017, 7(18), 11129–11134. https://doi.org/10.1039/c7ra00435d.

[20]. Immanuel, P., Senguttuvan, G., Chang, J. H., Mohanraj, K., & Kumar, N. S. Effect of Cr doping on Mn_3O_4 thin films for high-performance Supercapacitors. Journal of Materials Science: Materials in Electronics, 2021, 32(3), 3732–3742. https://doi.org/10.1007/s10854-020-05118-4.

[21]. K. Mohanraj, D. Balasubramanian, J. C. Synthesis and characterization of ruthenium-doped CdO nanoparticle and its n-RuCdO/p-Si junction diode application. Journal of Alloys and Compounds, 2019, 779, 762-775. https://doi.org/10.1016/j.jallcom.2018.11.264.

[22]. Said, L. Ben, Inoubli, A., Bouricha, B., & Amlouk, M. High Zr doping effects on the microstructural and optical properties of Mn_3O_4 thin films along with ethanol sensing. Spectrochimica Acta Part A: Molecular and Biomolecular Spectroscopy. 2017, 171, 487-498. https://doi.org/10.1016/j.saa.2016.08.014.

[23]. Shelke, A. R., Ghodake, G. S., Kim, D., Ghule, A. V, Kaushik, S. D., Lokhande, C. D., & Deshpande, N. G. Correlation of structural, transport and magnetic properties in $La_1\grave{A}_xZr_x$ MnO_3 manganite samples. Ceramics International, 2016, 42 (10), 12038-12045. https://doi.org/10.1016/j.ceramint.2016.04.131.

[24]. Sayyed, S. G., Shaikh, A. V., Dubal, D. P., & Pathan, H. M. Paving the Way towards Mn_3O_4 Based Energy Storage Systems. ES Energy & Environment, 2021, 14, 3–21. https://doi.org/10.30919/esee8c522.

[25]. Boukhachem, A., Boughalmi, R., Karyaoui, M., Mhamdi, A., Chtourou, R., Boubaker, K., & Amlouk, M. Study of substrate temperature effects on structural, optical, mechanical and opto-thermal properties of NiO sprayed semiconductor thin films. Materials Science and Engineering B: Solid-State Materials for Advanced Technology, 2014, 188, 72–77. https://doi.org/10.1016/j.mseb.2014.06.001.

[26]. Hosny, N. M., & Dahshan, A. Facile synthesis and optical band gap calculation of Mn_3O_4 nanoparticles. Materials Chemistry and Physics, 2012, 137(2), 637–643. https://doi.org/10.1016/j.matchemphys.2012.09.068.

[27]. Hanifehpour, Y., Mirtamizdoust, B., Cheney, M. A., & Joo, S. W. Facile synthesis, characterization and BET study of neodymium-doped spinel Mn_3O_4 nanomaterial with enhanced photocatalytic activity. Journal of Materials Science: Materials in Electronics, 2017, 28(16), 11654–11664. https://doi.org/10.1007/s10854-017-6968-5.

[28]. Maruthapandian, V., Pandiarajan, T., Saraswathy, V., & Muralidharan, S. Oxygen evolution catalytic behaviour of Ni doped Mn_3O_4 in alkaline medium. RSC Advances, 2016, 6(54), 48995–49002. https://doi.org/10.1039/C6RA01877G

[29]. Wang, T., Wang, L. X., Wu, D. L., Xia, W., & Jia, D. Z. Interaction between nitrogen and sulfur in co-doped graphene and synergetic effect in supercapacitor. Scientific Reports, 2015, 5, 1–9. https://doi.org/10.1038/srep09591.

[30]. Peng, D., Duan, L., Wang, X., & Ren, Y. Co_3O_4 composite nano-fibers doped with

[DOI: 10.22068/ijmse.3527]

Mn^{4+} prepared by the electro-spinning method and their electrochemical properties. RSC Advances, 2021, 11(39), 24125–24131. https://doi.org/10.1039/d0ra10336e

[31]. Fleischmann, S., Mitchell, J. B., Wang, R., Zhan, C., Jiang, D. E., Presser, V., & Augustyn, V. Pseudocapacitance: From Fundamental Understanding to High Power Energy Storage Materials. Chemical Reviews, 2020, 120(14), 6738–6782. https://doi.org/10.1021/acs.chemrev.0c00170.

[DOI: 10.22068/ijmse.3527]